ACS OMEGA

http://pubs.acs.org/journal/acsodf

Article

Efficient Mixing of Microfluidic Chip with a Three-Dimensional Spiral Structure

Junyao Wang, Xingyu Chen, Huan Liu,* Yunpeng Li, Tianhong Lang, Rui Wang, Bowen Cui, and Weihua Zhu*

Cite This: *ACS Omega* 2022, 7, 1527−1536

Read Online

ACCESS | Metrics & More | Article Recommendations

ABSTRACT: In this paper, a helical three-dimensional (3D) passive micromixer is presented. A three-dimensional spiral passive micromixer is fabricated through the 3D printing technology and the polymer dissolution technology. The main process is as follows: First of all, a high-impact polystyrene (HIPS) material was used to make a 3D spiral channel mold. Second, the channel mold was dissolved in limonene solvent. The mixing experiment shows that the single helix structure can improve the mixing efficiency to 0.85, compared with the mixing efficiency of 0.78 in the traditional T-shaped two-dimensional (2D)-plane channel. Different screw diameters, screw number structures, and flow rates are used to test the mixing effect. The optimal helical structure is 5 mm, and the flow rate is 2.0 mL/min. Finally, the mixing efficiency of the 3D helical micromixer can reach 0.948. The results show that the three-dimensional helical structure can effectively improve the mixing efficiency.

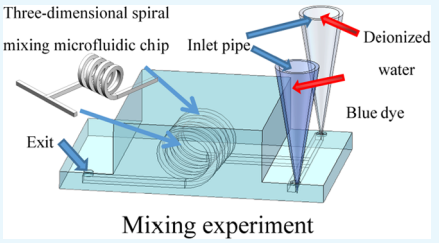

Mixing experiment

1. INTRODUCTION

Micromixer is widely used in micro/nanomanufacturing and is an important component in the microfluidic field.[1] It plays a key role in medical treatment, chemistry, and other fields.[2] The traditional micromixer is made of a planar single-layer structure.[3−5] Nowadays, with the improvement of 3D printing technology and the application of new materials, the production methods of micromixer are more diverse.[6]

At present, two-dimensional micromixers are also widely used,[7] such as X, Y, Z, and T passive micromixers.[8] The special protruding structure is convenient for processing, but the overall mixing efficiency is low. Fortunately, the invention relates to a nature-inspired mini-channel mixer by preparing a bionic structure mixer with improved mixing efficiency.[9] Nevertheless, its chips are too bulky. The plane network structure is too complicated, and it is very difficult to make. Noticeably, the utility model relates to an electroosmosis pressurized combined micromixer. The micromixer was made by 3D printing polylactic acid material.[10] The mixing efficiency was improved by electroosmosis pressurization on the basis of a two-dimensional structure. However, it requires extra resources. Remarkably, a lost-wax casting method was used to fabricate three-dimensional channels.[11] However, the molten wax preparation channel requires high-temperature conditions, and it is easy to leave residual. The resulting channel is of poor quality. Dramatically, the utility model relates to a three-dimensional micromixing ultrafast laser internal processing of glass,[12] which realizes a three-dimensional micromixer by laser processing of glass. However, the preparation process requires potassium hydroxide to be treated, which is dangerous. Importantly, the micromixer was fabricated by the fused deposition modeling (FDM) 3D printing technology.[13] The production cost is low, and the production time is fast. No more processing steps are required. Despite all of these, the actual use process needs to adopt the matching rotating platform. Noteworthily, the glass microfluidic system of monolithic 3D micromixer with impeller is proposed.[14] However, the impeller structure is complicated and the processing time is more than 24 h.

This paper presents a new micromixer with a three-dimensional helical structure. Combined with the 3D printing technology and the polymer dissolution technology, the micromixer with a 3D spiral channel can be directly manufactured without a bonding process. To improve the mixing efficiency of the mixer, the mixing efficiency of the mixer was investigated by simulating six kinds of structures. Then, the effects of three kinds of screw pitch and three kinds of screw numbers on mixing efficiency were verified by experiments. And the effect of flow velocity on the mixing efficiency of the six structures was verified.

2. MATERIALS AND METHODS

High-impact polystyrene (HIPS) and acrylonitrile butadiene styrene (ABS) were purchased from Flashforge, China. Sylgard

Received: November 11, 2021
Accepted: December 13, 2021
Published: December 21, 2021

https://doi.org/10.1021/acsomega.1c06352
ACS Omega 2022, 7, 1527−1536

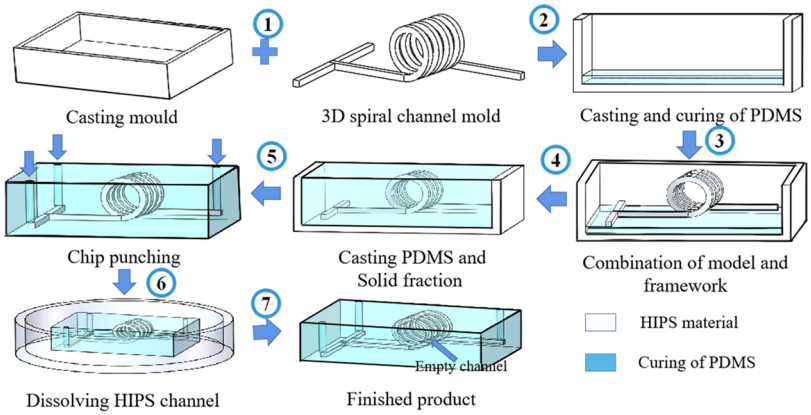

Figure 1. Schematic diagram of 3D helical micromixer.

Table 1. Manufacturing Steps and Data of 3D Spiral Micromixer

steps	production process	specific methods and parameters	time (min)
step 1	printing the ABS framework	3D printing technology is employed to fabricate the ABS framework with the size of 6 cm × 6 cm × 6 cm	5
step 2	printing the HIPS mold and casting the PDMS	HIPS material is printed into a three-dimensional helical structure. The cross-sectional size of the mold is 200 μm × 200 μm	20
		PDMS solution is poured with a thickness of 0.3 mm and cured at 80°	
step 3	placing the HIPS microchannel mold	HIPS mold is placed on the PDMS surface	20
		Heat curing is carried out at the temperature of 80°	
step 4	casting and curing	PDMS solution is poured with a thickness of 0.3 mm and cured at 80°	20
step 5	punching the holes	a punching device is used to punch holes on the chip, with a diameter of 2 mm	
step 6	dissolving the microchannel mold in limonene solvent	dissolved at a temperature of 100 °C and a limonene concentration of 50%	30
step 7	completing the chip	a micromixer with a three-dimensional spiral microchannel was fabricated	

Table 2. Accuracy Comparison between HIPS Die and Formed Channel

material	material properties	channel dimension	technology difficulty	scope of application
PMMA	low melting point and high optical properties	two	laser cutting chemical dissolution	not easy to process embrittlement
glass	high-pressure resistance and good thermal stability	two	lithographic chemical dissolution	complex structure and poor durability
silicon	poor optical properties and high hardness	two	curing light chemical dissolution	complex preparation and high cost
PDMS	high optical properties and high ductility	three	room-temperature curing chemical dissolution	without bonding flexible

184 silicone elastomer and curing agent were purchased from Dongguan Sanbang New Material Technology, China. A 3D printer (Flame, Flashforge) is employed to print pouring mold and microchannel mold with HIPS and ABS (Flashforge, China). Limonene solutions (Flashforge, China) are adopted to fabricate a microfluidic chip with the material of poly(dimethylsiloxane) (PDMS). An injection pump (LSP02-2B, Longerpump) is utilized to implement a mixing experiment. The cross section of the microchannel is observed based on an inverted fluorescence microscope (OLYMPUS IX73, Japan). The theoretical simulation software used in this paper is COMSOL5.6 software. The specific modules are the low-Reynolds-number turbulence module and the alkene material transfer module.

Figure 1 shows the fabrication schematic diagram of the 3D helical micromixer proposed in this paper. The specific production process and data are shown in Table 1. In the table, the time required for each step is presented. It is worth noting that due to the small size of the HIPS mold, the printing time is less than 1 min so step 2 takes 20 min.

A comparison was made with three materials,[15] as shown in Table 2. Among them, glass[16] and silicon[17] are adopted as chip materials, which have high-pressure resistance and good thermal stability. However, the production process requires photolithography and bonding technology, the manufacturing process is complex and costly, and the final chip has a complex structure and poor durability. Fortunately, the poly(methyl methacrylate) (PMMA) material[18,19] has the advantages of low melting point and high optical properties, but its production process requires laser cutting and bonding process, which cannot prepare conventional three-dimensional channels. The PDMS material used in this paper is integrated by curing. The monolithic chip requires no bonding. Therefore, the three-dimensional structure can be prepared and has certain flexibility compared with the other three materials and wider applicability.

3. RESULTS AND DISCUSSION

3.1. Mixing Efficiency of Planar and Three-Dimensional Structures. Figure 2 shows the mixing efficiency comparison diagram of a T-shaped channel[8] and a three-

https://doi.org/10.1021/acsomega.1c06352
ACS Omega 2022, 7, 1527−1536

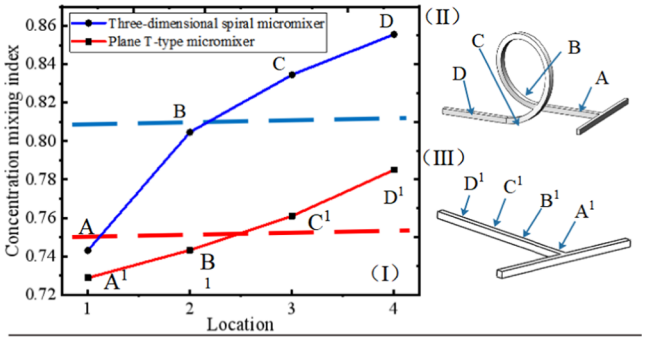

Micro mixer structure	Mixed efficiency at four locations			
	A/A^1	B/B^1	C/C^1	D/D^1
T-shaped microchannel	0.728	0.743	0.761	0.785
Spiral microchannel	0.743	0.804	0.834	0.856

Figure 2. (I) Line chart for a comparison of mixing efficiency between 3D helical structure and 2D T-shaped structure; (II) schematic diagram of three-dimensional spiral channel; (III) schematic diagram of two-dimensional T-channel; and (IV) comparison table of the mixing efficiencies of two structures.

position spiral channel, in which Figure 2(I) shows the mixing efficiency comparison diagram of two kinds of micromixer structures and Figure 2(II,III) shows the measurement points of two kinds of micromixer structures and their mixing efficiency. Ensure that the measuring points have the same length. In Figure 2(I), the average mixing index is taken, such as blue line and red line, where the average mixing efficiency of the three-position spiral channel is 0.809 and that of the planar T-shaped channel is 0.749. Figure 2 shows the specific mixing efficiency values at the relative positions of the two mixers. The mixing efficiency of the three-dimensional channel is generally about 12% higher than that of a two-dimensional channel. The same mixing efficiency is calculated by the following formula 1[20]

$$I = \left[1 - \frac{\sqrt{\frac{1}{N}\sum_{i=1}^{N}(X_i - \bar{X})^2}}{\sqrt{\frac{1}{N}\sum_{i=1}^{N}(X_{i-\text{unmix}} - \bar{X})^2}}\right] \times 100\% \quad (1)$$

where N is the number of selected points, X_i is the grayscale of the ith point on the cross section, $X_{i\text{-unmix}}$ is the grayscale of each point in the case of complete unmixing, and $\bar{X}$ is the average grayscale in the case of final mixing. Finally, the corresponding mixing efficiency value can be obtained. According to Figure 2(I), it can be seen that the mixing efficiency of the three-dimensional spiral micromixer is significantly improved compared with that of the T-channel micromixer, and the mixing efficiency of the two liquids can be achieved up to 85.6%. Because the spiral structure has a complex channel shape compared with the plane structure, when two kinds of liquids flow in the channel, the three-dimensional structure can lead to more drastic changes in the liquid flow, enhance the eddy current effect, and lead to stronger mixing effect. The results show that the three-dimensional helical structure has a stronger mixing performance than the planar T-shaped structure. It can be improved by 7.1% in the same length of the channel.

3.2. Hybrid Chip Simulation. *3.2.1. Simulation of Spiral Structure Channel.* Figure 3 shows the hybrid simulation diagram and local real experiment diagram of the two structures. Through the comparison of the two experiments and simulation screenshots, it can be seen that the main fluid form of the plane T-shaped mixer is laminar flow, where A, B, C, D, A^1, B^1, C^1, and D^1 are the simulation and physical drawings of the two-channel structures, respectively. The main fluid form of the three-dimensional spiral mixer is turbulence.[21,22] The mixing efficiency can be known by comparing the four positions. The four groups of positions are shown in Figure 2. In the end, the spiral structure has a better mixing effect. The T-channel structure involves the simulation equation as the Navier−Stokes eq 2[23]

$$\rho u \cdot \nabla u = -\nabla p + \nabla \cdot \mu(\nabla u + (\nabla u)^T) \quad (2)$$

where p is the density (kg/m^3), u is the velocity (m/s), and μ is the viscosity (N·s/m^2). By contrast, we can see that the helical structure with the final number of turns can reach the maximum mixing efficiency of 0.856. In this paper, the finite element method is used for hydrodynamic analysis. By dividing the computational area into grids, a network partition is carried out

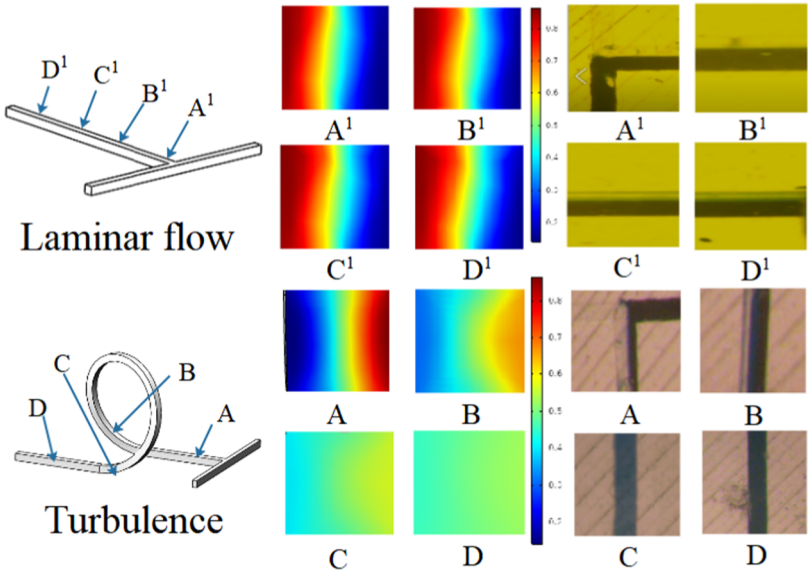

Figure 3. T-channel and spiral channel simulation and local physical map.

https://doi.org/10.1021/acsomega.1c06352
ACS Omega 2022, 7, 1527−1536

for a single helix structure. The specific table data are shown in Table 3.

Table 3. Numerical Model Detailed Information

property	value
mesh vertices	127 823
number of elements	169 900
minimum element quality	0.01068
average element quality	0.6054
element volume ratio	5.446×10^{-6}
mesh volume (mm^3)	11.27

There is a nonrepeating control volume around each grid point: a set of discrete equations is obtained by integrating the differential equations to be solved for each control volume. Three-dimensional discrete equations are used in this paper. Low Reynolds number $K-\varepsilon$ principle (eqs 3 and 4)

$$\frac{\partial(pk)}{\partial t} + \frac{\partial(pku_i)}{\partial x_i} = \frac{\partial}{\partial x_i}\left[\left(\mu + \frac{\mu_t}{\sigma_k}\right)\frac{\partial k}{\partial x_j}\right] + G_k - p\varepsilon - \left|2\mu\left(\frac{\partial k^{1/2}}{\partial n}\right)^2\right| \quad (3)$$

μ_t is the turbulent viscosity; n is the wall-normal coordinate; u is the flow rate; $C_{1\varepsilon}$, $C_{2\varepsilon}$, and C_μ are empirical constants; σ_k is the Prandtl number. The specific values are shown in Table 4. The

Table 4. Model Constant

$C_{1\varepsilon}$	$C_{2\varepsilon}$	C_μ	σ_k	σ_ε
1.44	1.92	0.09	1.0	1.3

governing equation diffusion coefficient includes turbulent diffusion coefficient and molecular diffusion coefficient. Turbulent Reynolds number should be introduced. On the basis of eq 3, model (4) is obtained by introducing coefficients f_1, f_2, f_3, and f_u.

$$\frac{\partial(p\varepsilon)}{\partial t} + \frac{\partial(p\varepsilon u_i)}{\partial x_i} = \frac{\partial}{\partial x_j}\left[\left(\mu + \frac{\mu_t}{\sigma_\varepsilon}\right)\frac{\partial \varepsilon}{\partial x_j}\right] + \frac{C_{1\varepsilon}\varepsilon}{k}G_k|f_1| - C_{2\varepsilon}p\frac{\varepsilon^2}{k}|f_2| + \left|2\frac{\mu\mu_1}{p}\left(\frac{\partial^2 u}{\partial n^2}\right)^2\right| \quad (4)$$

μ_t is the turbulent viscosity; n is the wall-normal coordinate; u is the flow rate; $C_{1\varepsilon}$, $C_{2\varepsilon}$, and C_μ are the empirical constants; and σ_k and σ_ε are the Prandtl number corresponding to turbulent kinetic energy k and dissipation rate ε, respectively. The constant values of the formula are shown in Table 4. G_k is the turbulent kinetic energy generation term caused by the average velocity gradient. Its calculation formula is shown in eq 5.

$$G_k = \mu\left\{2\left[\left(\frac{\partial u}{\partial x}\right)^2 + \left(\frac{\partial v}{\partial y}\right)^2 + \left(\frac{\partial w}{\partial z}\right)^2\right] + \left(\frac{\partial u}{\partial y} + \frac{\partial v}{\partial x}\right)^2 + \left(\frac{\partial u}{\partial z} + \frac{\partial w}{\partial x}\right)^2 + \left(\frac{\partial v}{\partial z} + \frac{\partial w}{\partial y}\right)^2\right\} \quad (5)$$

The coefficients f_1, f_2, f_3, and f_u are the modified parameters of the standard $K-\varepsilon$ equation. The present structure produces a low Reynolds number. Its calculation equation is shown in eq 6. The micromixer has a mixing channel width of 200 μm. The same design was adopted for the numerical modeling of the mixing process using COMSOL Multiphysics 5.6. The data of the developed experiments are shown in Table 5.

$$\begin{cases} f_1 \approx 1.0 \\ f_2 = 1.0 - 0.3\exp(-Re_t^2) \\ f_\mu = \exp(-2.5/(1 + Re_t/50)) \\ Re_t = pk^2/(\eta\varepsilon) \end{cases} \quad (6)$$

The coefficients f_1, f_2, f_3, and f_u are the modified parameters of the standard $K-\varepsilon$ equation. Re_t is a turbulent Reynolds number.

3.2.2. Simulation of a Spiral Structure Channel. Figure 4 shows the mixed simulation data of six different three-dimensional helical structures. Figure 4(I–III), respectively, shows the simulation mixing efficiency values with two, three, and four turns of screw structure. Figure 4(IV–VI), respectively, shows the simulation mixing efficiency values of 3, 4, and 5 mm screw diameters, where A, B, C, D, E, and F are three-dimensional schematic diagrams of six structures. Figure 4(VII) shows the simulation comparison diagram of the mixing efficiency trend of three different winding number structures. Figure 4(VIII) shows the comparative simulation trend chart of the mixing efficiency of three structures with different screw diameters. It is shown that the simulation mixing efficiency increases with the increase of the number of turns and screw diameter. The Navier–Stokes eq 1 is involved in the simulation.

The numerical definition parameters and boundary conditions involved in the simulation are shown in Tables 6 and 7. Table 6 shows the numerical simulation of boundary conditions. Table 7 shows the numerical simulation of variable parameters.

3.2.3. Velocity of Simulation. Figure 5(I–III), respectively, shows the ratio of simulation mixing efficiencies of two, three, and four turns of helical structure at four different flow rates. Figure 5(IV–VI) shows the ratio of simulation mixing efficiency

Table 5. Numerical Simulation of Variable Parameters

parameter	value					
channel cross section (μm^2)	4	4	4	4	4	4
Re	0.011, 0.023, 0.036, 0.047	0.011, 0.023, 0.036, 0.047	0.011, 0.023, 0.036, 0.047	0.011, 0.023, 0.036, 0.047	0.011, 0.023, 0.036, 0.047	0.011, 0.023, 0.036, 0.047
traffic	0.5, 1.0, 1.5, 2.0	0.5, 1.0, 1.5, 2.0	0.5, 1.0, 1.5, 2.0	0.5, 1.0, 1.5, 2.0	0.5, 1.0, 1.5, 2.0	0.5, 1.0, 1.5, 2.0
traffic than	8, 4, 3, 2	8, 4, 3, 2	8, 4, 3, 2	8, 4, 3, 2	8, 4, 3, 2	8, 4, 3, 2
channel intercept	3	3	3	3	4	5
number of coils	2	3	4	4	4	4

https://doi.org/10.1021/acsomega.1c06352
ACS Omega 2022, 7, 1527–1536

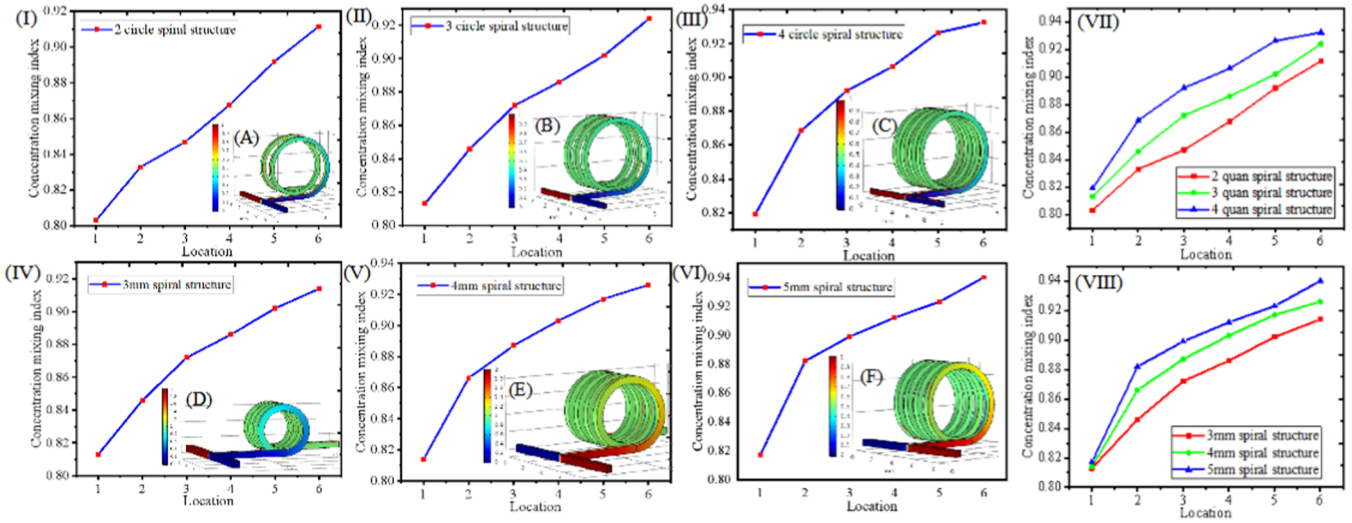

Figure 4. Mixed simulation data of six different 3D helical structures.

Table 6. Numerical Simulation of Boundary Conditions

	entry 1	entry 2	exit	spiral wall surface
flow field	$P = 0$	$P = 0$	$P = 0$	$u = 0$
ion concentration field	$C_1 = 1$ mol/m^3	$C_2 = 2$ mol/m^3		$n = 0$

Table 7. Numerical Simulation of Variable Parameters

serial number	cross-sectional area of the channel	number of turns	spiral diameter	viscosity coefficient
1	200 μm × 200 μm	2	4	8.55×10^{-4}
2		3	4	
3		4	4	
4		4	3	
5		4	4	
6		4	5	

of three kinds of helical diameter structures at four flow rates. The simulation set velocity is shown in Table 8, and the final simulation results show that the mixing efficiency increases with the increase of the velocity. When the screw diameter is 5 mm and the flow rate is 2 L/min, a maximum mixing efficiency of 0.95 can be achieved.

3.3. Chip Mixing Experiment. *3.3.1. Effects of Different Screw Diameters on Mixing Efficiency.* Figure 6 reveals the mixing efficiency curves of the three screw diameters. Figure 6(I–III), respectively, proves the mixing efficiency values of helical structures with 3, 4, and 5 mm diameters. The 3D figure exhibits the 3D schematic diagram of the corresponding structure and the measuring position of mixing efficiency. After this, Figure 6(IV) indicates the trend comparison of the mixing efficiency of the three structures. In the end, Figure 6(V) provides the comparison of the final mixing efficiency values of the three structures. It is concluded that the mixing efficiency increases with the increase of winding number. The 5 mm diameter spiral structure can achieve the maximum mixing efficiency of 0.91. When the fluid passes through the channel and reaches the starting position of the spiral, turbulence occurs. As the screw diameter increases, the structure through which the fluid flows changes more, which is conducive to destroying the intermolecular force. Therefore, when the fluid moves in the spiral structure, increasing the contact angle of the fluid can fully destroy the intermolecular force inside the fluid. Finally, it is concluded that the mixing efficiency of the 5 mm helical structure is higher. It can reach 0.91. According to the kinetic energy principle $K-\varepsilon$ at a low Reynolds number (eqs 7–10)

$$P_k = \mu_T\left(\nabla u: (\nabla u + (\nabla u)^T) - \frac{2}{3}(\nabla \cdot u)^2\right) - \frac{2}{3}pk\nabla \cdot u \tag{7}$$

$$f_\mu = (1 - e^{-l^*/14})^2 \cdot \left(1 + \frac{5}{R_t^{3/4}} e^{-(R_t/200)^2}\right) \tag{8}$$

$$l^* = (pu_\varepsilon l_W)/\mu \tag{9}$$

$$\mu_T = pf_\mu C_\mu \frac{k^2}{\varepsilon} \tag{10}$$

where ep is the turbulence dissipation rate; p is the stress; μ is the viscosity; Δ is the gradient operator; ρ is the density; μ_T is the eddy viscosity; l^* is the radius coefficient; and l_w is the radius of the spiral. It can be seen that with the increase of radius, the radius coefficient increases and the eddy viscosity increases, and finally the kinetic energy mixing efficiency improves. It can be seen from Figure 6(V) that the turbulent kinetic energy increases with the increase of flow velocity. The flow is accelerated, creating a prolongation effect that further mixes the flow layer and improves the mixing quality.

3.3.2. Different Circle Number Affects Mixing Efficiency. Figure 7 indicates the mixing efficiency curves of the three winding numbers. As can be seen, Figure 7(I–III) proves the mixing efficiency values of 2-turn, 3-turn, and 4-turn spiral structures, respectively, and the 3D map demonstrates the 3D schematic diagrams of the corresponding three structures and the measuring positions of mixing efficiency. Then, Figure 7(IV) shows the trend comparison of the mixing efficiency of the three structures. Finally, Figure 7(V) provides the final mixing efficiency values of the three structures and the comparison of channel parameters. It is shown that the mixing efficiency increases with the increase of winding number. The mixing efficiencies of the three helical structures were 0.87, 0.88, and 0.90, respectively. When the fluid passes through the channel and reaches the starting position of the spiral, turbulence occurs.

https://doi.org/10.1021/acsomega.1c06352
ACS Omega 2022, 7, 1527–1536

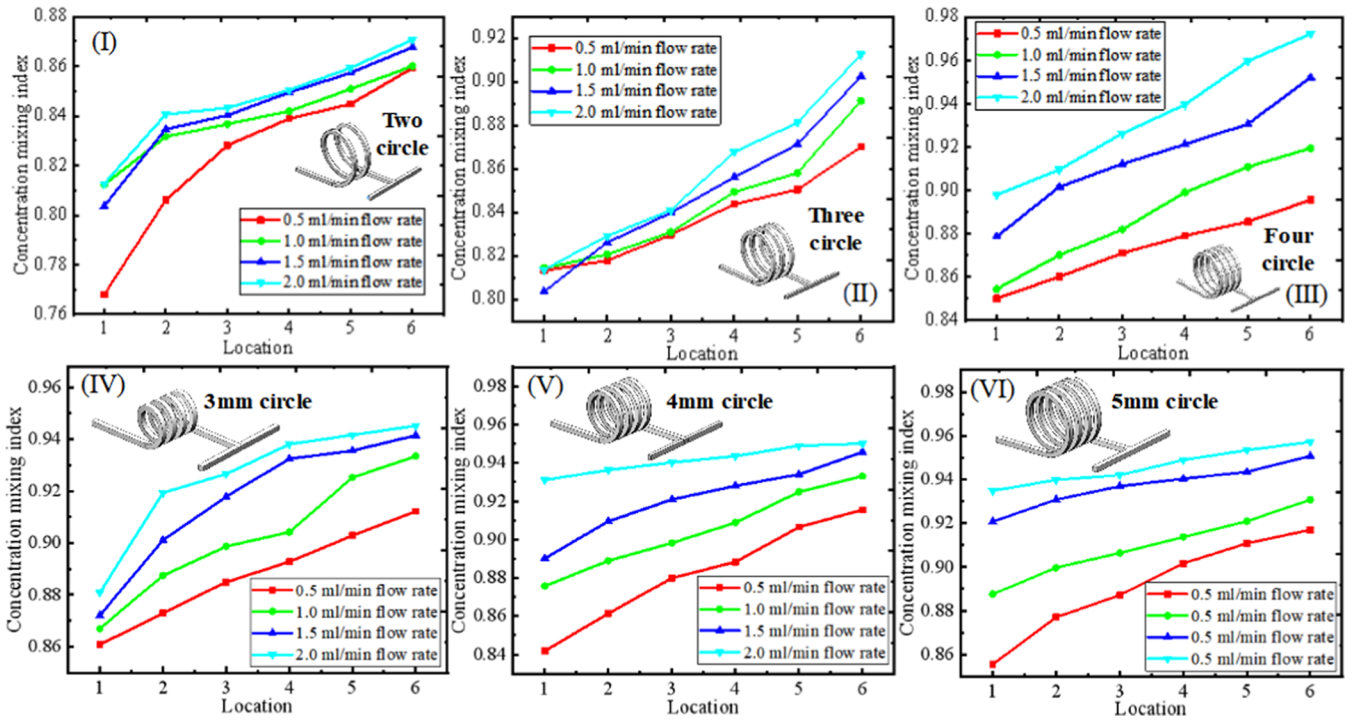

Figure 5. Comparison of mixing efficiencies of six different three-dimensional helical structures at four flow rates.

Table 8. Numerical Simulation of Variable Parameters

serial number	structure	velocity
1	2 laps	0.5 mL/min, 1.0 mL/min, 1.5 mL/min, 2.0 mL/min
2	3 laps	0.5 mL/min, 1.0 mL/min, 1.5 mL/min, 2.0 mL/min
3	4 laps	0.5 mL/min, 1.0 mL/min, 1.5 mL/min, 2.0 mL/min
4	3 mm	0.5 mL/min, 1.0 mL/min, 1.5 mL/min, 2.0 mL/min
5	4 mm	0.5 mL/min, 1.0 mL/min, 1.5 mL/min, 2.0 mL/min
6	5 mm	0.5 mL/min, 1.0 mL/min, 1.5 mL/min, 2.0 mL/min

Therefore, when the fluid moves in the helical structure and passes through more helical structures, the intermolecular force within the fluid can be fully destroyed. Finally, it is concluded that the mixing efficiency of the four-loop spiral structure is higher. It can reach 0.90.

3.3.3. Comparison of Mixing Efficiency at Different Flow Rates. Figure 8 demonstrates the mixing efficiency curves of three winding numbers at different flow rates. As can be seen, Figure 8(I–IV) reveals the mixing efficiency values of two, three,

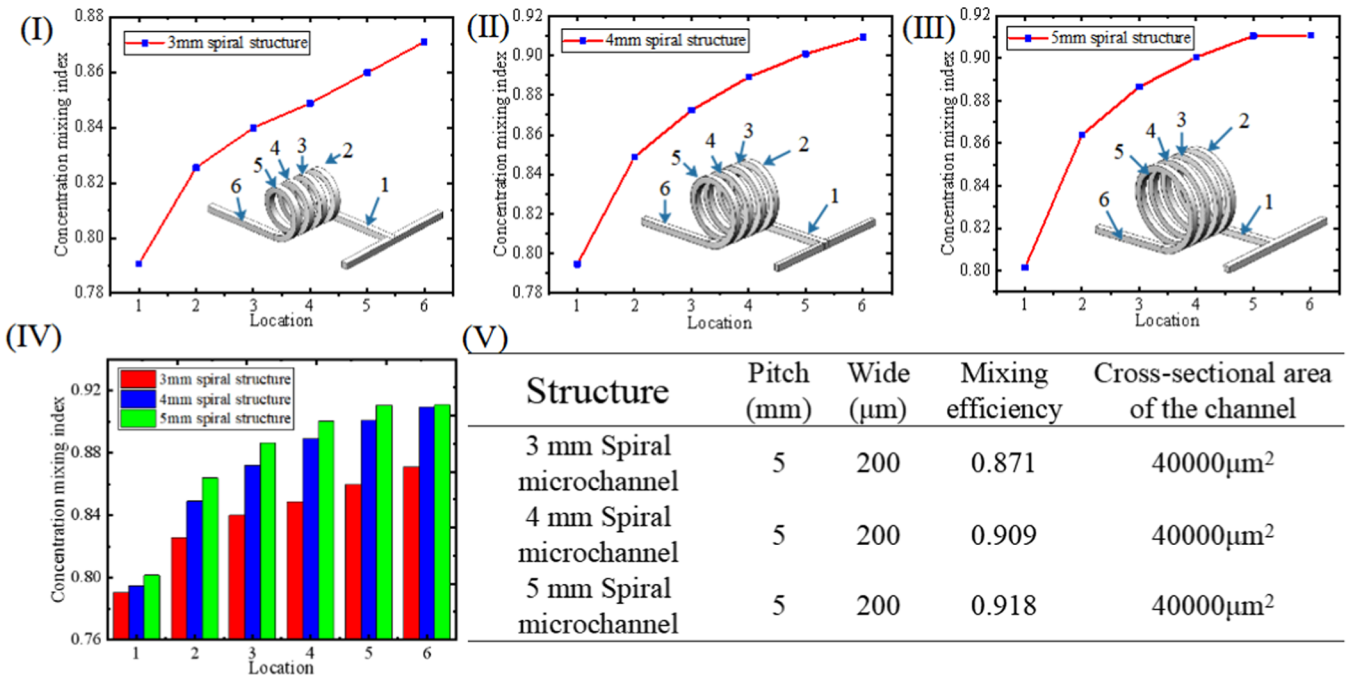

(V)

Structure	Pitch (mm)	Wide (μm)	Mixing efficiency	Cross-sectional area of the channel
3 mm Spiral microchannel	5	200	0.871	40000μm^2
4 mm Spiral microchannel	5	200	0.909	40000μm^2
5 mm Spiral microchannel	5	200	0.918	40000μm^2

Figure 6. Mixing efficiency curves of three kinds of helical diameters.

https://doi.org/10.1021/acsomega.1c06352
ACS Omega 2022, 7, 1527−1536

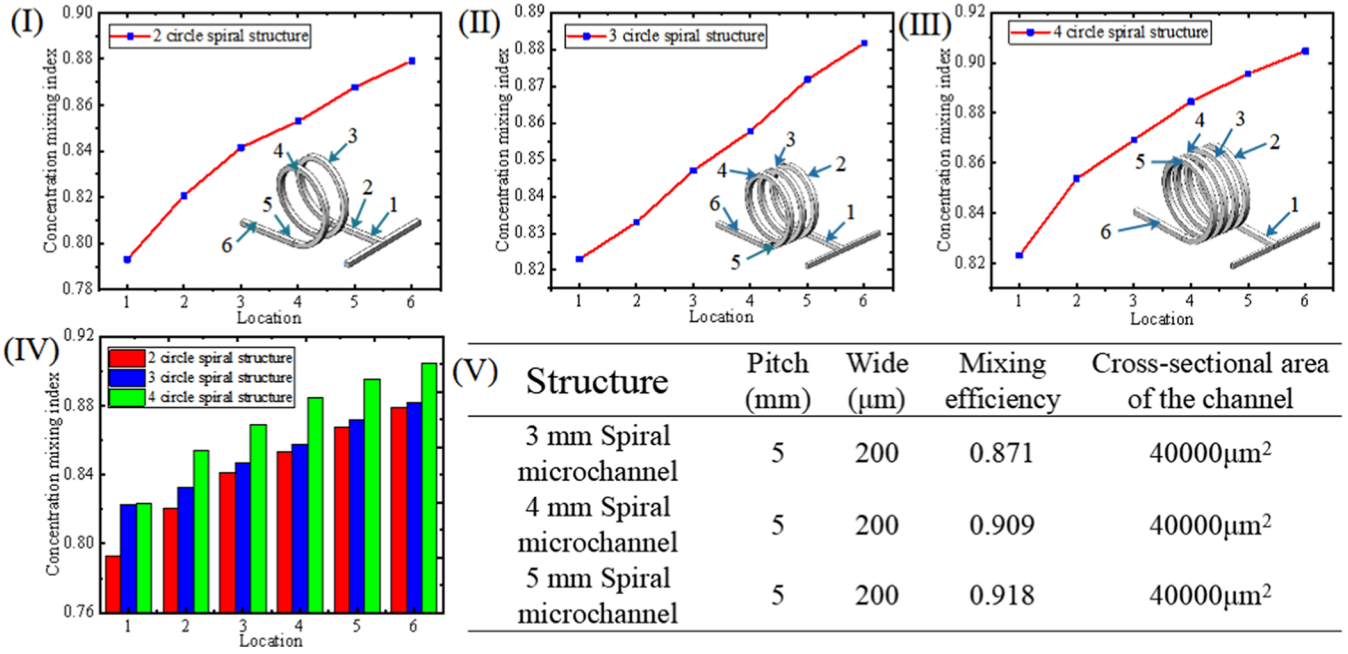

(V)

Structure	Pitch (mm)	Wide (μm)	Mixing efficiency	Cross-sectional area of the channel
3 mm Spiral microchannel	5	200	0.871	40000μm^2
4 mm Spiral microchannel	5	200	0.909	40000μm^2
5 mm Spiral microchannel	5	200	0.918	40000μm^2

Figure 7. Three kinds of winding number mixing efficiency curve.

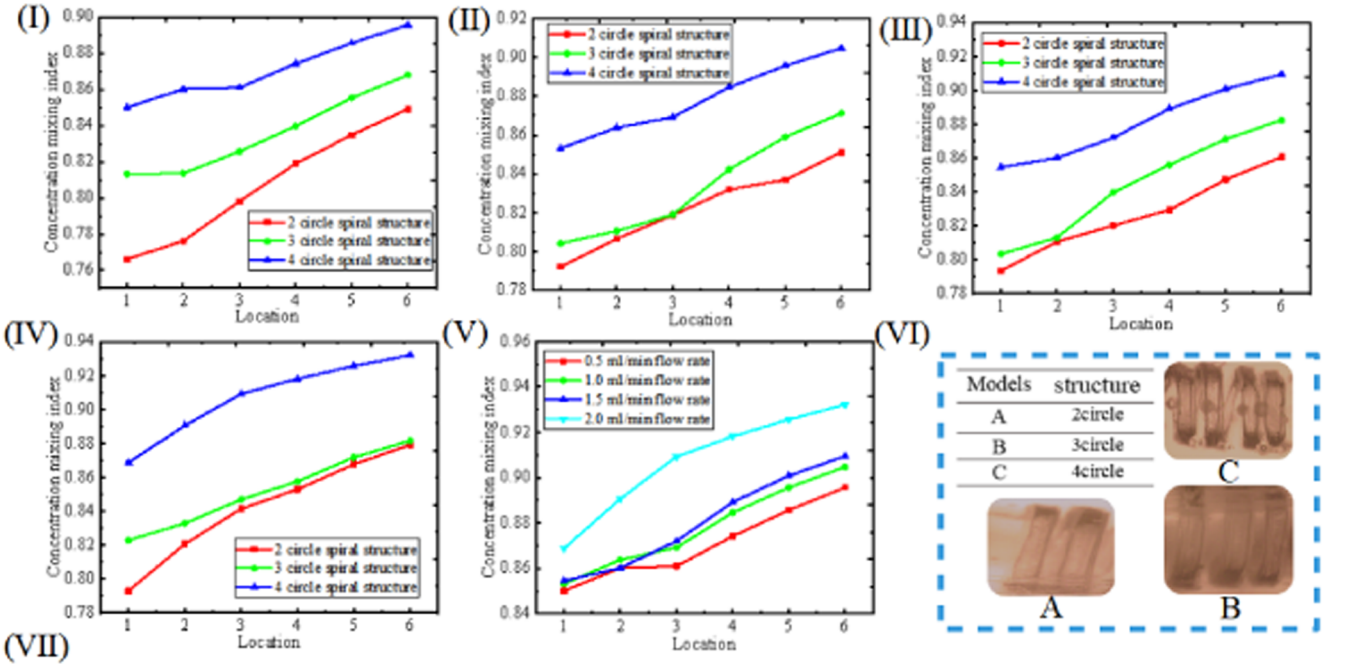

Structure	Channel width (μm)	Spiral length (mm)	Hybrid materials	Flow velocity/Mixing efficiency **0.5ml/min**	Flow velocity/Mixing efficiency **1.0ml/min**	Flow velocity/Mixing efficiency **1.5ml/min**	Flow velocity/Mixing efficiency **2.0ml/min**
2 circle Spiral microchannel	200	25.12	Deionized water and blue dye	0.84925	0.85111	0.86066	0.87924
3 circle Spiral microchannel	200	37.68		0.86801	0.87125	0.88246	0.88157
4 circle Spiral microchannel	200	50.24		0.89564	0.90474	0.90947	0.93215

Figure 8. Mixing efficiency curves of three kinds of turn numbers at different flow rates and the real picture.

https://doi.org/10.1021/acsomega.1c06352
ACS Omega 2022, 7, 1527−1536

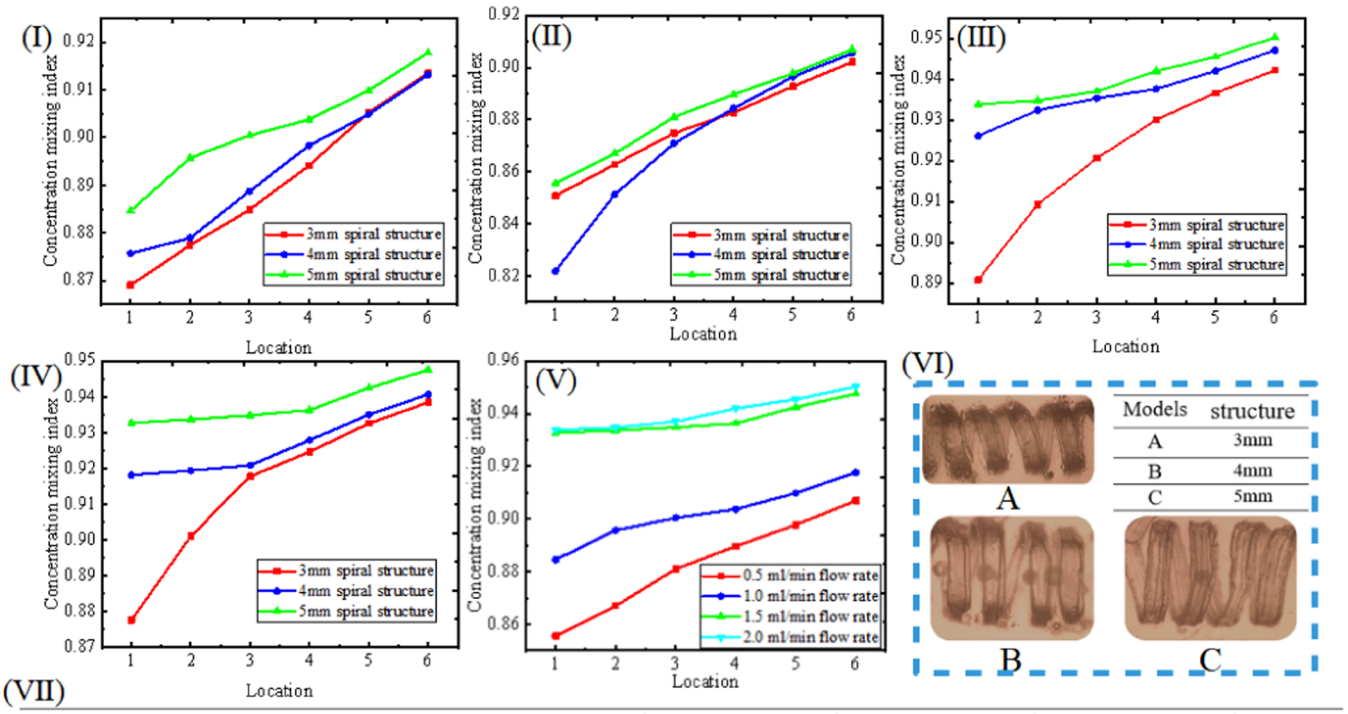

Structure	Channel width (μm)	Spiral length (mm)	Hybrid materials	Flow velocity/Mixing efficiency **0.5ml/min**	Flow velocity/Mixing efficiency **1.0ml/min**	Flow velocity/Mixing efficiency **1.5ml/min**	Flow velocity/Mixing efficiency **2.0ml/min**
3mm Spiral microchannel	200	37.68	Deionized water and blue dye	0.90216	0.91349	0.93847	0.94217
4mm Spiral microchannel	200	50.24		0.90551	0.91314	0.9407	0.94708
5mm Spiral microchannel	200	62.8		0.90699	0.91772	0.94754	0.95022

Figure 9. Mixing efficiency curves of three kinds of pitch at different flow rates and real pictures.

Table 9. Comparison of Different Micromixers

production methods	material	important technological process	make available	production cost	channel dimension	channel quality
surface modification adhesion	PDMS- glass (PDMS)	room-temperature high-pressure chemical etching surface modification bonding	50 min	expensive	two	inferior
lost-wax casting	wax and PDMS	3D-printed wax materials 130 °C dissolving		cheap	three	inferior
laser processing	glass	laser processing chemical etching bonding	over 24 h	expensive	three	good
FDM 3D printing technology	ABS material	FDM 3D printing integral molding	2 h	general	three	ropy
3D printing solution	HIPS limonene solution	3D printing solution without bonding	30 min	cheap	three	good

and four turns of helical structures at different flow rates, respectively. According to Figure 8(V), the mixing efficiency trend comparison diagram of three winding numbers at four flow rates is presented. Figure 8(VI) proves the actual micrograph and size table of the three structures. The table in Figure 8(VII) demonstrates channel size, mixed materials, and the corresponding final mixing efficiency at four flow rates. With the increase of flow velocity, the pressure strength of the fluid in the helical structure increases; meanwhile, the intermolecular force of the fluid is accelerated and destroyed. Furthermore, the frequency of eddy currents forming the small area of fluid inside the spiral channel increases and then the mixing efficiency increases. As a consequence, the mixing efficiency of the spiral channel is improved with the increase of the flow velocity. Finally, the maximum mixing efficiency of the four-loop helical structure is 0.93 under the condition of 2.0 mL/min.

Figure 9 shows the mixing efficiency curves of three kinds of pitch at different flow rates. As can be seen from Figure 9(I–IV), with the increase of screw diameter (from 3 to 5 mm), the mixing efficiency increases from 0.90 to 0.90. Simultaneously, it can be seen from Figure 9(V) that the turbulent kinetic energy increases with the increase of flow velocity. The accelerated flow is creating a prolongation effect that further mixes the flow layer and improves the mixing quality. The mixing efficiency ranges from 0.90 to 0.95. To sum up, the 5 mm helical structure can reach the maximum mixing efficiency of 0.95 under the

https://doi.org/10.1021/acsomega.1c06352
ACS Omega 2022, 7, 1527−1536

condition of 2.0 mL/min flow rate. Figure 9(VI) shows the physical drawing and size table under the microscope. The table in Figure 9(VII) shows channel size, mixed materials, and the corresponding final mixing efficiency at four flow rates.

3.4. Comparison of Different Micromixers. With the progress of micromixer preparation methods,[24,25] this paper compares four micromixer production methods as shown in Table 9. For example, the surface modification method can only be used to fabricate the micromixer in two dimensions.[26] In view of this, a lost-wax casting method was used to fabricate three-dimensional channels.[11] However, it needs a high temperature to prepare a 3D channel by melting wax, which will affect the channel forming. It is notable that a uniform three-dimensional micromixing mixer is used to process glass by laser processing. The mixer channel is of good quality. But even so, this process takes more than 24 h. It is worth mentioning that low-cost FDM printers manufacture micromixers. The micromixer was fabricated by the FDM 3D printing technology.[10] Its production time is reduced to 2 h. However, the production process requires the use of special equipment. It is not easy to prepare on a large scale. Fortunately, a 3D helical micromixer using 3D printing and polymer dissolution technology has been studied in this paper. It has the advantages of simple manufacturing method, short preparation time, and the ability to prepare complex 3D helical structures.

4. CONCLUDING REMARKS

A method of a three-dimensional helical micromixer with the advantages of high mixing efficiency and high complexity level of the structure is introduced in this paper. The conclusions are as follows:

A Compared with that of the T-shaped straight channel with the same length and cross-sectional area of the channel, the mixing efficiency of the three-dimensional single helical channel increases from 0.78 to 0.85. Consequently, compared with the planar structure, the three-dimensional spiral structure can increase the mixing efficiency.

B Under the premise of the same cross-sectional area, the mixing efficiency can be increased by adding the spiral structure. Specifically, the mixing efficiencies of the two-loop spiral structure, the three-turn helical structure, and the four-loop helical structure are 0.88, 0.89, and 0.91 respectively.

C Under the same number of turns, the influence of pitch on the mixing efficiency of the 3D helical micromixer is obtained. Among them, the mixing efficiencies are 0.88, 0.89, and 0.92 for 3, 4, and 5 mm diameters, respectively. It is concluded that increasing the diameter of the spiral structure can increase the mixing efficiency of the micromixer.

D According to the low Reynolds number $K-\varepsilon$ principle, mixing efficiency experiments are carried out with different structures and different flow rates. It is concluded that the mixing efficiency of both structures increased with the increase of flow rate. The mixing efficiency of different turn numbers can reach 0.93 eventually. The mixing efficiency of helical structures with different diameters can reach 0.946.

In conclusion, compared with the conventional planar structure, the micromixer proposed in this paper can effectively improve the mixing efficiency. Finally, the micromixer has the best mixing performance when the screw diameter is 5 mm and the flow rate is 2.0 mL/min.

AUTHOR INFORMATION

Corresponding Authors

Huan Liu − *School of Mechanical Engineering, Northeast Electric Power University, Jilin 132012, China;* orcid.org/0000-0003-3580-7907; Email: 20192850@neepu.edu.cn

Weihua Zhu − *Jilin Technology College of Electronic Information, Jilin 132021, China*; Email: jdzyzwh@163.com

Authors

Junyao Wang − *School of Mechanical Engineering, Northeast Electric Power University, Jilin 132012, China*

Xingyu Chen − *School of Mechanical Engineering, Northeast Electric Power University, Jilin 132012, China*

Yunpeng Li − *School of Mechanical Engineering, Northeast Electric Power University, Jilin 132012, China*

Tianhong Lang − *School of Mechanical Engineering, Northeast Electric Power University, Jilin 132012, China*

Rui Wang − *School of Mechanical Engineering, Northeast Electric Power University, Jilin 132012, China*

Bowen Cui − *School of Mechanical Engineering, Northeast Electric Power University, Jilin 132012, China*

Complete contact information is available at: https://pubs.acs.org/10.1021/acsomega.1c06352

Funding

This project was supported by the National Natural Science Foundation of China (grant no. 51505077), Project Agreement for Science and Technology Development of Jilin Province (JJKH20200105KJ), and Science and Technology Innovation Development Project of Jilin City (201750230, 20166013, 20166012).

Notes

The authors declare no competing financial interest.

The data supporting the findings of this study are available from the corresponding author upon reasonable request.

REFERENCES

(1) Agarwal, A.; Salahuddin, A.; Wang, H.; Ahamed, M. J. Design and development of an efficient fluid mixing for 3D printed lab - on - a - chip. *Microsyst. Technol.* **2020**, *26*, 2465−2477.

(2) Baki, A.; Löwa, N.; Remmo, A.; Wiekhorst, F.; Bleul, R. Micromixer Synthesis Platform for a Tuneable Production of Magnetic Single-Core Iron Oxide Nanoparticles. *Nanomaterials* **2020**, *10*, No. 1845.

(3) Hong, S. O.; Park, K. S.; Kim, D. Y.; Lee, S. S.; Lee, C. S.; Kim, J. M. Gear-shaped micromixer for synthesis of silica particles utilizing inertio-elastic flow instability. *Lab Chip* **2021**, *21*, 513−520.

(4) Xiong, S.; Chen, X.; Chen, H.; Chen, Y.; Zhang, W. Numerical study on an electroosmotic micromixer with rhombic structure. *J. Dispersion Sci. Technol.* **2021**, *42*, 1331−1337.

(5) Zhang, N.; Zha, K.; Wang, J. Exploring the Design Efficiency of Random Microfluidic Mixers. *IEEE Access* **2021**, *9*, 9864−9872.

(6) Raza, W.; Hossain, S.; Kim, K. Y. A review of passive micromixers with a comparative analysis. *Micromachines* **2020**, *11*, No. 455.

(7) Su, T.; Cheng, K.; Wang, J.; Xu, Z.; Dai, W. A fast design method for passive micromixer with angled bend. *Microsyst. Technol.* **2019**, *25*, 4391−4397.

(8) Mariotti, A.; Antognoli, M.; Galletti, C.; Mauri, R.; Salvetti, M. V.; Brunazzi, E. The role of flow features and chemical kinetics on the reaction yield in a Tshaped micro-reactor. *Chem. Eng. J.* **2020**, *396*, No. 125223.

(9) Tarlet, D.; Fan, Y.; Luo, L. Design and mixing performance characterization of a mini-channel mixer with nature-inspired geometries. *Chem. Eng. Res. Des.* **2020**, *164*, 230−239.
(10) Wang, Y.; Zhang, Y.; Qiao, Z.; Wang, W. A 3D Printed Jet Mixer for Centrifugal Microfluidic Platforms. *Micromachines* **2020**, *11*, No. 695.
(11) Tachibana, D.; Matsubara, K.; Matsuda, R.; Furukawa, T.; Maruo, S.; Tanaka, Y.; Fuchiwaki, O.; Ota, H. 3D Helical Micromixer Fabricated by Micro Lost-Wax Casting. *Adv. Mater. Technol.* **2020**, *5*, No. 1900794.
(12) Li, W.; Chu, W.; Yin, D.; Liang, Y.; Wang, P.; Qi, J.; Wang, Z.; Lin, J.; Wang, M.; Wang, Z.; Cheng, Y. A three-dimensional microfuidic mixer of a homogeneous mixing efciency fabricated by ultrafast laser internal processing of glass. *Appl. Phys. A* **2020**, *126*, No. 816.
(13) Martinez-López, J. I.; Cervantes, H. A. B.; Iturbe, L. D. C.; Vázquez, E.; Naula, E. A.; López, A. M.; Siller, H. R.; Mendoza-Buenrostro, C.; Rodríguez, C. A. Characterization of Soft Tooling Photopolymers and Processes for Micromixing Devices with Variable Cross-Section. *Micromachines* **2020**, *11*, No. 970.
(14) Kim, S.; Kim, J.; Joung, Y. H.; Ahn, S.; Park, C.; Choi, J.; Koo, C. Monolithic 3D micromixer with an impeller for glass microfluidic systems. *Lab Chip* **2020**, *20*, 4474−4485.
(15) Pattanayak, P.; Singh, S. K.; Gulati, M.; Vishwas, S.; Kapoor, B.; Chellappan, D. K.; Anand, K.; et al. Microfuidic chips: recent advances, critical strategies in design, applications and future perspectives. *Microfluid. Nanofluid.* **2021**, *25*, No. 99.
(16) Han, Y.; Jiao, Z.; Zhao, J.; Chao, Z.; You, Z. A simple approach to fabricate multi-layer glass microfuidic chips based on laser processing and thermocompression bonding. *Microfluid. Nanofluid.* **2021**, *25*, No. 77.
(17) Lebedev, D.; Malyshev, G.; Ryzhkov, I.; Mozharov, A.; Shugurov, K.; et al. Focused ion beam milling based formation of nanochannels in silicon-glass microfluidic chips for the study of ion transport. *Microfluid. Nanofluid.* **2021**, *25*, No. 51.
(18) Kotz, F.; Mader, M.; Dellen, N.; Risch, P.; Kick, A.; Helmer, D.; Rapp, B. E. Fused Deposition Modeling of Microfluidic Chips in Polymethylmethacrylate. *Micromachines* **2020**, *11*, No. 873.
(19) Zhang, S.; Shin, Y. C. Effective methods for fabricating trapezoidal shape microchannel of arbitrary dimensions on polymethyl methacrylate (PMMA) substrate by a CO2 laser. *Int. J. Adv. Manuf. Technol.* **2017**, *93*, 1079−1094.
(20) Mashaei, P. R.; Asiaei, S.; Hosseinalipour, S. M. Mixing efficiency enhancement by a modified curved micromixer; a numerical study. *Chem. Eng. Process.* **2020**, *154*, No. 108006.
(21) Oevreeide, I. H.; Zoellner, A.; Mielnik, M. M.; Stokke, B. T. Curved passive mixing structures: a robust design to obtain efficient mixing and mass transfer in microfluidic channels. *J. Micromech. Microeng.* **2021**, *31*, No. 015006.
(22) Pourabed, A.; Younas, T.; Liu, C.; Shanbhag, B. K.; He, L. Z.; Alan, T. High throughput acoustic microfluidic mixer controls self-assembly of protein nanoparticles with tuneable sizes. *J. Colloid Interface Sci.* **2021**, *585*, 229−236.
(23) Wang, J. Y.; Liu, C.; Xu, Z.; Li, Y. K.; Liu, Y. L. Ion-enrichment and ion-depletion of nanochannels based on electrochemical potential in a micro-nanofluidic chip. *Microsyst. Technol.* **2014**, *20*, 35−39.
(24) Jain, S.; Unni, H. N. Numerical modeling and experimental validation of passive microfluidic mixer designs for biological applications. *AIP Adv.* **2020**, *10*, No. 105116.
(25) Dehghani, T.; Moghanlou, F. S.; Vajdi, M.; Asl, M. S.; Shokouhimehr, M.; Mohammadi, M. Mixing enhancement through a micromixer using topology optimization. *Chem. Eng. Res. Des.* **2020**, *161*, 187−196.
(26) Wang, J. Y.; Xu, Z. Electrokinetic ion breakdown in a nanochannel. *AIP Adv.* **2016**, *6*, No. 075025.

https://doi.org/10.1021/acsomega.1c06352
ACS Omega 2022, 7, 1527−1536